Received: 24 August 2017 | Revised: 12 February 2018 | Accepted: 13 February 2018
DOI: 10.1002/ardp.201700272

FULL PAPER

DPhG ARCH PHARM
Archiv der Pharmazie

Pyridine-substituted thiazolylphenol derivatives: Synthesis, modeling studies, aromatase inhibition, and antiproliferative activity evaluation

Merve Ertas[1] | Zafer Sahin[1] | Barkin Berk[1] | Leyla Yurttas[2] | Sevde N. Biltekin[3] | Seref Demirayak[1]

[1] Department of Pharmaceutical Chemistry, School of Pharmacy, İstanbul Medipol University, İstanbul, Turkey

[2] Faculty of Pharmacy, Department of Pharmaceutical Chemistry, Anadolu University, Eskisehir, Turkey

[3] Department of Pharmaceutical Microbiology, School of Pharmacy, İstanbul Medipol University, İstanbul, Turkey

Correspondence
Merve Ertas, Department of Pharmaceutical Chemistry, School of Pharmacy, İstanbul Medipol University, Kavacık street no. 19, 34810 İstanbul, Turkey.
Email: mertas@medipol.edu.tr

Funding information
Anadolu University Scientific Research Projects Commission, Grant number: 1410S422

Abstract

Drugs used in breast cancer treatments target the suppression of estrogen biosynthesis. During this suppression, the main goal is to inhibit the aromatase enzyme that is responsible for the cyclization and structuring of estrogens either with steroid or non-steroidal-type inhibitors. Non-steroidal derivatives generally have a planar aromatic structure attached to the triazole ring system in their structures, which inhibits hydroxylation reactions during aromatization by coordinating the heme group. Bioisosteric replacement of the triazole ring system and development of aromatic/cyclic structures of the side chain can increase the selectivity for aromatase enzyme inhibition. In this study, pyridine-substituted thiazolylphenol derivatives, which are non-steroidal triazole bioisosteres, were synthesized using the Hantzsch method, and physical analysis and structural determination studies were performed. The IC_{50} values of the compounds were determined by a fluorescence-based aromatase inhibition assay. Then, their antiproliferative activities on the MCF7 and HEK 293 cell lines were evaluated with the 3-(4,5-dimethylthiazol-2-yl)-2,5-diphenyltetrazolium bromide (MTT) assay. Furthermore, the crystal structure of human placental aromatase was subjected to a series of docking experiments to identify the possible interactions between the most active structure and the active site. Lastly, an *in silico* technique was performed to analyze and predict the drug-likeness, molecular and ADME properties of the synthesized molecules.

KEYWORDS
anticancer activity, aromatase, breast cancer, MCF-7, non-steroidal inhibitor

1 | INTRODUCTION

Breast cancer is the most common cancer among women worldwide.[1] Most breast cancers in postmenopausal women are estrogen receptor positive (ER^+)[2,3] and adjuvant endocrine therapy has an important role in treating this type. Efficacy of suppression treatment is based on the idea that estrogens stimulate the growth of residual cancer cells or contribute to the initiation of a new primary cancer over time. Selective estrogen-receptor modulators (SERMs) and aromatase inhibitors (AIs) are two basic regimes used in clinics.

During the final step of estrogen biosynthesis, the aromatase enzyme plays a crucial role by both enhancing the aromatic feature of

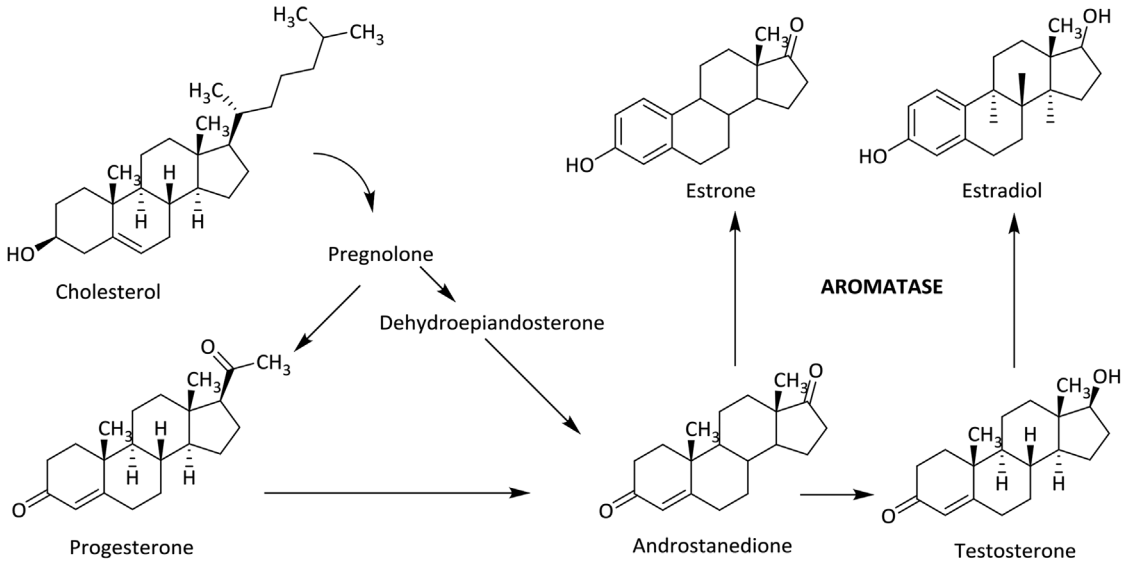

FIGURE 1 Key role of aromatase in the estrogen pathway

androstenedione/testosterone and eliminating a methyl group from the ring system.[4,5] Therefore, inhibition of aromatase with AIs is a promising method of developing new solutions (Figure 1).[6,7]

In the last few decades, three generations of AIs have been developed. Those that are most preferred in clinical therapy are third-generation AIs since they have more favorable tolerability profiles and they are more selective and/or potent compared with first- and second-generation agents.[8,9] In terms of chemistry and pharmacology, there are two broad categories of third-generation AIs[10]; reversible non-steroidal agents consist of anastrozole and letrozole (triazole derivatives), and irreversible steroidal inhibitors comprise exemestane and formestane.[11] Recent studies on breast cancer treatment involve non-steroidal inhibition of the aromatase enzyme rather than steroidal therapy[12–14] due to the prolonged inactivating effect of irreversible steroidal agents on the enzyme even after the drug is cleared from circulation. In this case, continuation of estrogen production depends on the synthesis of new aromatase molecules.[15]

Resveratrol (3,5,4′-trihydroxy-*trans*-stilbene) is a stilbenoid, which can modulate several steps in carcinogenesis; however, it has several negative effects and disadvantages in clinical use.[16] Research involving the addition of central 1,3-thiazole or 1,3,5-thiadiazole systems and changing phenolic rings with the pyridine ring within this structure has resulted in improvement of aromatase inhibitory activity (Figure 2).[16–19]

In the current study, we prepared 18 non-steroidal pyridine-substituted thiazolylphenol derivatives for the purpose of inhibiting the active site of aromatase cytochrome P450. Aromatase inhibitory activities of the molecules were measured by a fluorescence-based assay using ketoconazole as standard. Then, antiproliferative and anticancer activities of the compounds were evaluated with an MTT assay over the human breast adenocarcinoma (MCF7) and human embryonic kidney (HEK 293) cell lines. Further interactions between the active molecule and the active site of the enzyme was analyzed through docking experiments using the crystal structure of human placental aromatase cytochrome P450 in complex with androstenedione (3EQM).[7] Furthermore, absorption, distribution, metabolism, and excretion (ADME), drug-likeness, and molecular properties of all the molecules were predicted by *in silico* techniques. Although compounds **2** and **4–8** had been previously synthesized using different methods and investigated in other subjects such as chemiluminescence,[20–26] we resynthesized them and performed enzymatic and cellular experiments to test their activities.

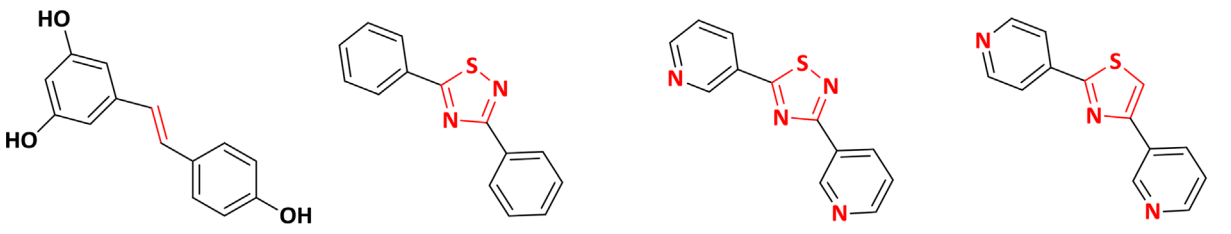

FIGURE 2 Aromatase inhibition of resveratrol and analogs[17–19]

2 | RESULTS AND DISCUSSION

2.1 | Chemistry

A synthetic pathway consists of a two-step reaction. In the first step, 1-(substituted phenyl)ethanone derivatives were brominated using copper(II) bromide in ethyl acetate resulting in 2-bromo-1-(substituted phenyl)ethanones. For these types of bromination reactions, acetic-acid medium is generally used[27]; however, in the current study, copper(II) bromide was preferred since in acetic medium, structures containing phenolic parts can direct the bromine to be substituted over the ring system. In the second step, through the Hantzsch thiazole[28] synthesis, 2-bromo-1-(substituted phenyl)ethanones and various pyridinethioamides were reacted in ethanol to obtain either 2/3/4-[2-(pyridin-2/3/4-yl)thiazol-4-yl]phenol or 4-substituted-2-[2-(pyridin-2/3/4-yl)thiazol-4-yl]phenol structured compounds with yields ranging from 65 to 82% (Figure 3).

In the IR spectra, all the compounds had a strong C—O stretching band for the phenol group at 1200 cm^{-1}. The ^{1}H NMR spectra of the compounds showed that the protons belonging to the hydroxyl group differed between 9.55 and 11.4 ppm according to their substitution position. The only hydrogen of the central thiazole was found to be a singlet between 8.0 and 8.75 ppm. The other aromatic hydrogens of both phenol and pyridine rings ranged from 6.9 to 8.9 ppm. All the remaining protons were observed according to the expected chemical shift and integral values. In the ^{13}C NMR spectra, the carbons of the phenol, thiazole, and pyridine ring systems were observed at 116–129, 162–191, and 150–155 ppm, respectively. The molecular ion peaks (M^{+}) of the compounds confirmed their molecular weights.

2.2 | Biological activity

2.2.1 | Aromatase enzyme inhibitory activity

Aromatase inhibitory activities of compounds **1–18** and ketoconazole (IC_{50} = 0.95 μM) were determined within a concentration range of 10 μM–4.5 nM. Most efficient molecules were found to be compounds **3** (IC_{50} = 1.84 μM), **6** (IC_{50} = 0.91 nM), **8** (IC_{50} = 1.51 μM), **9** (IC_{50} = 0.96 μM), **10** (IC_{50} = 1.25 μM), **12** (IC_{50} = 1.62 μM), **13** (IC_{50} = 1.74 μM), and **16** (IC_{50} = 1.38 μM). These results are shown in Table 1 and Figure 4.

TABLE 1 The IC_{50} values[a] of aromatase-active compounds (10 μM–4.5 nM)

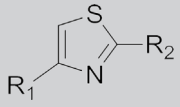

Compound	R_1	R_2	IC_{50} (μM)
1	2-OH Phenyl	2-Pyridinyl	12.68 ± 0.23
2	2-OH Phenyl	3-Pyridinyl	9.63 ± 2.13
3	2-OH Phenyl	4-Pyridinyl	**1.84 ± 0.20**
4	3-OH Phenyl	2-Pyridinyl	2.86 ± 0.44
5	3-OH Phenyl	3-Pyridinyl	8.87 ± 1.33
6	3-OH Phenyl	4-Pyridinyl	**0.9 ± 1.12**[b]
7	4-OH Phenyl	2-Pyridinyl	7.92 ± 3.06
8	4-OH Phenyl	3-Pyridinyl	**1.51 ± 0.35**
9	4-OH Phenyl	4-Pyridinyl	**0.96 ± 0.44**
10	2-OH-5-CH_3 Phenyl	2-Pyridinyl	**1.25 ± 0.62**
11	2-OH-5-CH_3 Phenyl	3-Pyridinyl	15.49 ± 0.44
12	2-OH-5-CH_3 Phenyl	4-Pyridinyl	**1.62 ± 0.11**
13	2-OH-5-OCH_3 Phenyl	2-Pyridinyl	**1.74 ± 0.18**
14	2-OH-5-OCH_3 Phenyl	3-Pyridinyl	11.63 ± 4.70
15	2-OH-5-OCH_3 Phenyl	4-Pyridinyl	10.35 ± 1.18
16	2-OH-5-Cl Phenyl	2-Pyridinyl	**1.38 ± 0.31**
17	2-OH-5-Cl Phenyl	3-Pyridinyl	7.39 ± 3.13
18	2-OH-5-Cl Phenyl	4-Pyridinyl	9.48 ± 3.82
KTZ[c]			0.95 ± 0.09

[a]The values represent mean ± SD of triplicate determinations.
[b]The IC_{50} value of compound **6** and its SD were both in nM units.
[c]Ketoconazole (KTZ) was used as standard for aromatase.
The bold values displays meaningful results according to the standard.

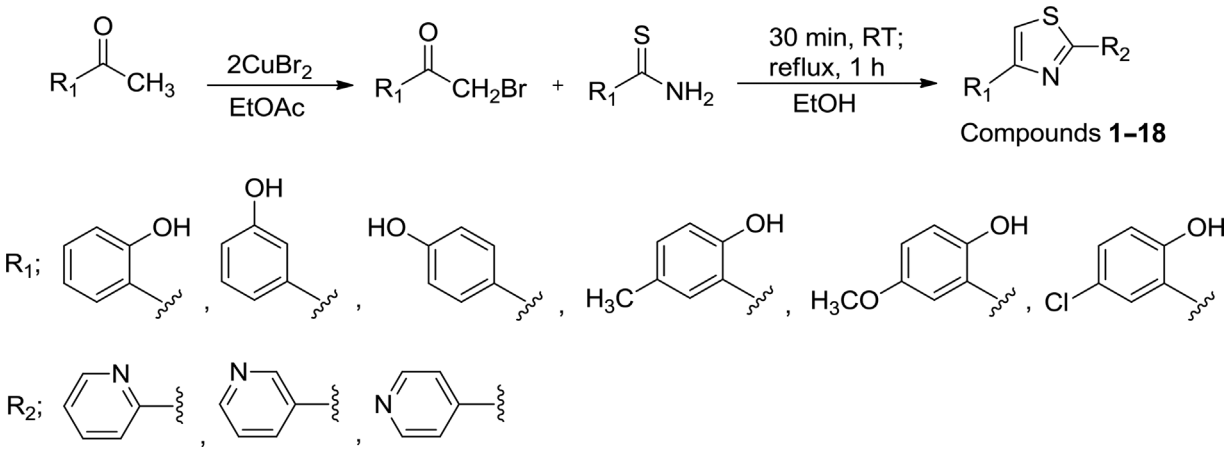

FIGURE 3 General synthesis and structures of the synthesized compounds

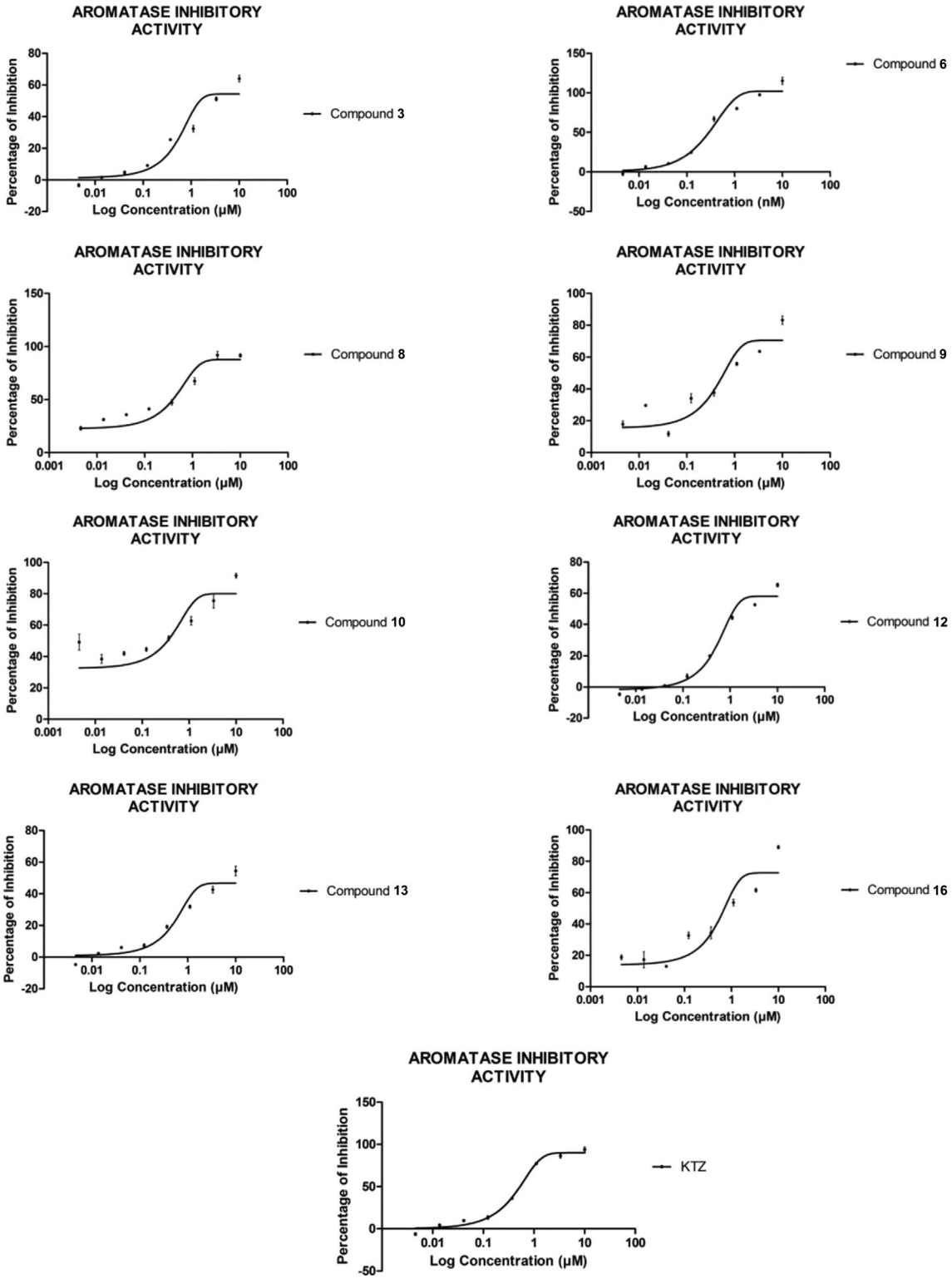

FIGURE 4 Dose–response curves for compounds **3**, **6**, **8–10**, **12**, **13**, and **16** and ketoconazole

As shown in Table 1, compound **6** inhibited the enzyme at 1000 times lower concentration compared to ketoconazole. In addition, the efficacy of compound **9** was very similar to that of ketoconazole.

2.2.2 | Anticancer activity against tumor and normal cells in culture

The 10^{-4} M concentrations of compounds were tested on MCF7 and HEK 293 cell lines for measuring the viability of the exposed cells.

Synthesized compound **13** exhibited the highest cytotoxic activities against MCF7 cells (56.44%), the lowest proliferative activities against HEK 293 cells (10.86%). Compound **14** had the most cytotoxic activity on MCF7 (68.32%), so this compound showed the most potent anticancer activity. Compounds **13** (56.44%), **16** (49.58%), **8** (47.67%), and **10** (46.09%) were more active than the others. Compound **6** that had the highest anti-aromatase activity had a toxic effect on MCF7; however, its activity was 10% less compared to HEK 293. Compounds **14** and **15** showed cytotoxic effects on both the HEK 293 and MCF7 cell lines. The obtained values are listed in Figure 5 and Table 2.

2.3 | Molecular modeling studies

2.3.1 | Docking studies

The lowest IC_{50} value during aromatase inhibition was obtained from compound **6**; therefore, a docking experiment was undertaken with this compound and to determine 3EQM in order to identify the interaction pattern between the active site and the compound. The experiment was initially performed using the XP algorithm of Glide, treating the receptor as rigid and the ligands as flexible. The docking protocol had the same constraints as a previous study detailing high throughput docking to find potent azole compounds as aromatic nitrogen heterocycles that are able to inhibit P450 enzymes by coordinating the heme iron atom, thus preventing oxygen binding and the subsequent oxidation reaction of the substrate.[29,30] A van der Waals radius scaling factor of 0.50 for atoms with a partial atomic charge (absolute value) less than 0.15 was used to soften the potential for the non-polar parts of the receptor. The enclosing box was centered on the heme residue, and default sizes were used for both the enclosing and bounding boxes. A metal constraint was used to determine ligand poses where an aromatic nitrogen atom interacts with the heme iron. The ligand nitrogen must be within 2.4 Å of the metal in order to satisfy the constraint. To validate the experiment, anastrozole, a non-steroidal aromatase inhibitor which interacts with the enzyme through a triazole moiety, was first docked to check whether the binding mode was consistent with the available data. After achieving a successful repetition of the results, the experiment was performed with compound **6**. Then, the experiment was improved with the induced-fit protocol of Glide, in which both receptor and ligand were simulated as flexible. The overall settings of this protocol were also the same as described by Caporuscio et al.[29] with the only exception being the initial use of the XP protocol, rather than SP. The ligand seemed to fit well into the pocket similar to anastrazole where the pyridine ring system was coordinated with heme moiety (Figure 6).

Nitrogen atom of the pyridine system acted as an H-bond acceptor from the Thr 310 side chain. This part of the molecule was in hydrophobic interactions with Ala 306 and Val 370 of the active site. Other active site amino acids that stabilized the ligand with hydrophobic interactions were Val 373, Leu 372, Met 374, Leu 228, Phe 116, and Trp 224. These amino acids surrounded the phenolic part of the molecule producing a small hydrophobic cavity. Furthermore, this phenolic part had a π–π stacking interaction with Phe 134. A similar kind of stacking was also observed between the thiazole part and Arg 115.

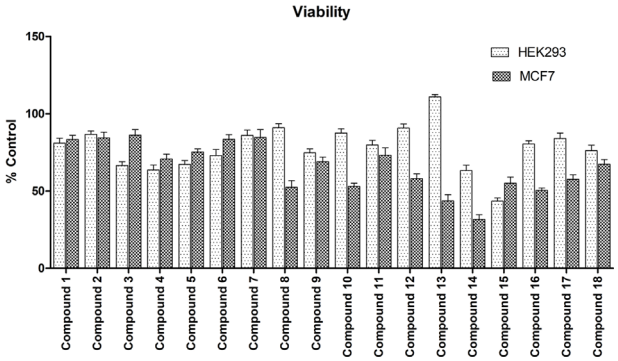

FIGURE 5 Effect of compounds **1–18** at the concentration of 10^{-4} M on the viability of MCF7 and HEK 293 cells

TABLE 2 % Viability values (10^{-4} M) for compounds in MCF7 and HEK 293 cell lines

MCF7		HEK 293	
Compound	% Control	Compound	% Control
1	83.39 ± 2.64	**1**	80.94 ± 3.21
2	84.40 ± 3.60	**2**	86.69 ± 2.08
3	86.12 ± 2.51	**3**	66.41 ± 2.51
4	70.81 ± 3.05	**4**	63.60 ± 3.21
5	75.24 ± 2.00	**5**	67.19 ± 2.51
6	83.44 ± 3.05	**6**	72.89 ± 4.04
7	84.71 ± 4.93	**7**	85.93 ± 3.51
8	52.33 ± 4.35	**8**	90.86 ± 2.64
9	68.96 ± 3.05	**9**	74.73 ± 2.51
10	53.01 ± 2.00	**10**	87.51 ± 2.64
11	73.22 ± 4.72	**11**	79.74 ± 3.00
12	58.02 ± 3.05	**12**	90.69 ± 2.64
13	43.56 ± 4.04	**13**	110.86 ± 1.52
14	31.68 ± 3.05	**14**	63.23 ± 3.51
15	55.03 ± 4.00	**15**	43.49 ± 2.00
16	50.42 ± 1.52	**16**	80.46 ± 2.08
17	57.51 ± 3.00	**17**	83.95 ± 3.60
18	67.28 ± 3.05	**18**	76.15 ± 3.51

2.3.2 | Prediction of drug-likeness, molecular and ADME properties

In this study, the drug-likeness, molecular and ADME properties of all the compounds were calculated using the QikProp function of Maestro (Schrödinger 2016-4). All the compounds showed promising findings presenting with a drug-like/lead-like profile according to their #stars rankings. The combinations of the HOA values being 3, %HOA of all

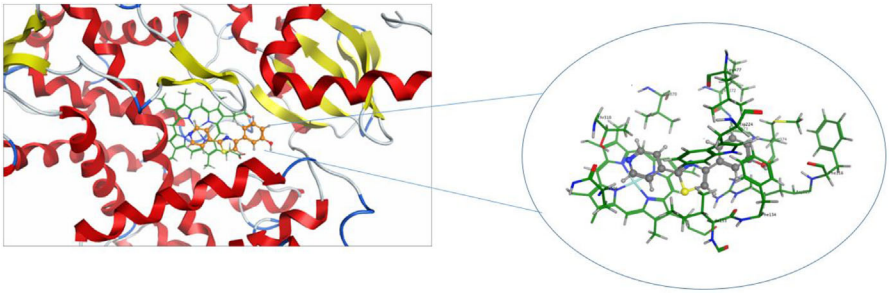

FIGURE 6 Positioning of compound **6** docked with the induced-fit protocol in the active site and compound **6** in the active site of aromatase

compounds being 100%, and all PCaco values being very high indicated that these compounds are suitable for oral use. The log K_p values varying between −1.80 (compounds **5**, **6**, **8**, and **9**) and −1.07 (compound **1**) indicate that these compounds can be effectively used in topical preparations. Furthermore, the logarithm of the predicted binding constant to human serum albumin of the selected compounds, i.e., the log K_{HSA} values, varied between 0.08 (compounds **2** and **3**) and 0.33 (compound **10**). It is important to note that the binding of drugs to plasma proteins such as human serum albumin, lipoprotein, glycoprotein, α, β, and γ globulins greatly reduces the quantity of the drug in general blood circulation. In other words, the less bound a drug is, the more efficiently it can traverse cell membranes or diffuse. The log K_{HSA} values showed that these derivatives could freely circulate and easily traverse cell membranes. The logHERG values of the compounds predicted with the *in silico* method were between −5.38 (compound **15**) and −5.64 (compounds **4** and **7**). The HERG K^+ channel, best known for its impact on the electrical activity of the heart by synchronizing beating activity, appears to be the molecular target responsible for the cardiac toxicity of a wide range of therapeutic drugs.[31] HERG has also been found associated with modulating the functions of certain cells of the nervous system and with establishing and maintaining cancer-like features in leukemic cells.[32] Thus, HERG K^+ channel blockers are potentially toxic and IC_{50} values often provide reasonable predictions for the cardiac toxicity of drugs in the early stages of drug discovery.[33] The results showed the presence of a mild risk of compounds acting as HERG K^+ channel blockers. As a basic rule, polar drugs cannot easily penetrate the BBB. The blood/brain partition coefficient (logBB) [−0.20 (compounds **5**, **6**, **8**, and **9**) to 0.29 (compound **16**)], PMDCK [1216.28 (compound **8**) and 7046.34 (compound **16**)], and logPo/w [2.82 (compounds **5** and **6**) and 3.70 (compound **16**)] values are useful for determining the penetration capacity of a compound from BBB. The values predicted for these parameters of the synthesized compounds were within the ranges defined for 95% of drugs. Moreover, the predicted CNS value of the compounds with a maximum of 1 indicated mild to medium activity.

Although the predictive results must be checked with actual experiments, the activity studies showed that compounds **3**, **6**, **8**–**10**, **12**, **13**, and **15** exhibited very promising IC_{50} values during aromatase and cellular inhibition assays. Using a thiazole ring system instead of a double bond in resveratrol and the 1,3,5-thiadiazole systems worked extremely well with the insertion of pyridine and phenol to both sides of the molecule. Such improvements with these structures can lead to more effective oral non-steroidal aromatase inhibitors with less cytotoxicity to healthy human cells.

3 | EXPERIMENTAL

3.1 | Chemistry

3.1.1 | General

All the chemicals were purchased from Aldrich Chemical Co. (Steinheim, Germany). Melting points were determined with a Stuart melting point apparatus SMP30 (Staffordshire, UK). IR spectra (KBr) were recorded on a PerkinElmer Spectrum Two FT-IR spectrometer (Waltham, MA, USA) and ^{1}H NMR spectra were obtained by Bruker DPX-500, 500 MHz High Performance Digital FT-NMR. ^{13}C NMR spectra were measured using a DPX-125, 125 MHz High Performance Digital FT-NMR. All the chemical shift values were recorded as δ (ppm). Mass spectra were obtained using an Agilent 1100 MSD series mass spectrometer. The purity of the compounds was checked by thin-layer chromatography on silica gel-coated aluminum sheets (Merck, 1.005554, silica gel HF254–361, Type 60, 0.25 mm; Darmstadt, Germany). Elemental analyses were performed with a Leco CHNS 932 analyzer (Leco Corp., MI, USA) and were found to be within ±0.4% of the theoretical values for C, H, and N.

The InChI codes of the investigated compounds together with some biological activity data are provided as Supporting Information.

3.1.2 | General procedure for the synthesis of 2-bromo-1-(substituted phenyl)ethanone compounds

1-(Substituted phenyl)ethanone derivatives (0.1 mol) and $CuBr_2$ (0.2 mol) were mixed in ethyl acetate and refluxed for 6–8 h until the green color disappeared. The mixtures were cooled and kept refrigerated overnight for the total precipitation of CuBr. The precipitates were filtered and the ethyl acetate phases were extracted with water (2 × 100 mL) to remove all the inorganic leftovers. Then, the ethyl acetate phase was dried with anhydrous sodium sulfate, filtered, and concentrated in a vacuum to yield target compounds.

3.1.3 | General procedure for the synthesis of 2/3/4-[2-(pyridin-2/3/4-yl)thiazol-4-yl]phenol and 4-substituted-2-[2-(pyridin-2/3/4-yl)thiazol-4-yl]-phenol compounds

Equimolar appropriate amounts of pyridinethioamides (3.6 mmol) and 2-bromo-1-(substituted phenyl)ethanone derivatives were mixed and stirred in ethanol (50 mL) at room temperature for 30 min followed by refluxing for an hour. The mixtures were cooled to 0°C and the precipitates collected through filtration were dissolved in water and treated with 1 M sodium acetate solution. New precipitates were collected by filtration, dried, and recrystallized from ethanol or an ethanol/water (1:1) mixture.

2-[2-(Pyridin-2-yl)thiazol-4-yl]phenol (1)

Yield: 76%, mp: 124.3°C, IR υmax (cm^{-1}): 3104–3039 (aromatic C—H), 1247 (C—O). ^{1}H NMR (500 MHz) (DMSO-d_6) δ (ppm): 6.95 (t, 1H, J: 7.50 Hz, *J* = 7.50 Hz, Ph), 7.01 (d, 1H, *J* = 8.13 Hz, Ph), 7.23 (t, 1H, *J* = 7.64 Hz, Ph), 7.54 (dd, 1H, *J* = 7.49 Hz, *J* = 4.66 Hz, Py), 8.02 (t, 1H, *J* = 7.72 Hz, *J* = 7.72 Hz, Py), 8.17 (d, 1H, *J* = 7.7, Ph), 8.25 (d, 1H, *J* = 7.213 Hz, Py), 8.31 (s, 1H, Th), 8.68 (dd, 1H, *J* = 4.68 Hz, *J* = 0.6 Hz, Py), 10.56 (s, 1H, OH). ^{13}C NMR: 116.98, 119.43, 119.77, 120.121, 125.72, 129.05, 129.73, 138.33, 150.27, 150.71, 153.17, 155.53, 167.29. For $C_{14}H_{10}N_2OS$ calcd. 66.12% C, 3.96% H, 11.02% N; found: 66.08% C, 3.96% H, 11.08% N. Mass (ESI), *m/z*: 255 (M+1).

2-[2-(Pyridin-3-yl)thiazol-4-yl]phenol (2)

Yield: 67%, mp: 134.1°C, IR υmax (cm^{-1}): 3120–3000 (aromatic C—H), 1248 (C—O). ^{1}H NMR (500 MHz) (DMSO-d_6) δ (ppm): 6.95 (t, 1H, *J* = 7.49 Hz, *J* = 7.49 Hz, Ph), 7.01 (d, 1H, *J* = 8.08 Hz, Ph), 7.21–7.25 (m, 1H, Ph), 7.59 (dd, 1H, *J* = 4.83 Hz, *J* = 7.99 Hz, Ph), 8.19 (d, 1H, *J* = 7.79 Hz, Py), 8.32 (s, 1H, Th), 8.39–8.41 (m, 1H, Py), 8.71 (d, 1H, *J* = 4.79 Hz, Py), 9.22 (d, 1H, *J* = 1.64 Hz, Py), 10.55 (s, 1H, OH). ^{13}C NMR: 116.94, 119.43, 119.78, 120.13, 124.78, 129.29, 129.31, 129.81, 134.14, 147.45, 151.47, 152.97, 155.53, 162.95. For $C_{14}H_{10}N_2OS$ calcd. 66.12% C, 3.96% H, 11.02% N; found: 66.05% C, 3.98% H, 11.03% N. Mass (ESI), *m/z*: 255 (M+1).

2-[2-(Pyridin-4-yl)thiazol-4-yl]phenol (3)

Yield: 69%, mp: 131°C, IR υmax (cm^{-1}): 3131.3–2856.8 (aromatic C—H), 1279.58 (C—O). ^{1}H NMR (500 MHz), (DMSO-d_6) δ (ppm): 6.96 (t, 1H, *J* = 7.47 Hz, *J* = 7.47 Hz, Ph), 7.02 (d, 1H, *J* = 8.07 Hz, Ph), 7.24 (t, 1H, *J* = 7.64 Hz, *J* = 7.65 Hz, Ph), 7.97 (d, 2H, *J* = 5.4 Hz, Py), 8.19 (dd, 1H, *J* = 1.35 Hz, *J* = 7.79 Hz, Ph), 8.38 (s, 1H, Th), 8.74 (d, 2H, Py), 10.55 (s, 1H, OH). ^{13}C NMR: 116.94, 119.33, 119.81, 120.56, 129.36, 129.29, 129.31, 129.36, 129.92, 139.87, 151.24, 153.31, 155.55, 163.29. For $C_{14}H_{10}N_2OS$ calcd. 66.12% C, 3.96% H, 11.02% N; found: 66.11% C, 3.92% H, 11.01% N. Mass (ESI) *m/z*: 255 (M+1).

3-[2-(Pyridin-2-yl)thiazol-4-yl]phenol (4)

Yield: 82%, mp: 172.4°C, IR υmax (cm^{-1}): 3133.3 (aromatic C—H), 1235.02 (C—O). ^{1}H NMR (500 MHz) (DMSO-d_6) δ (ppm): 6.82 (dd, 1H, *J* = 2.21 Hz, *J* = 7.95 Hz, Ph), 7.29 (t, 1H, *J* = 7.85, *J* = 7.85 Hz, Ph), 7.48–7.50 (m, 1H, Ph), 7.50–7.53 (m, 2H, Py and Ph), 8.01 (td, 1H, *J* = 1.53 Hz, *J* = 7.72 Hz, *J* = 7.72 Hz, Py), 8.17 (s, 1H, Th), 8.24 (d, 1H, *J* = 7.87, Py), 8.66 (d, 1H, *J* = 4.78, Th), 9.57 (s, 1H, OH). ^{13}C NMR: 113.49, 115.82, 117.27, 117.41, 119.69, 125.65, 130.31, 135.72, 138.24, 150.20, 150.91, 156.22, 158.27, 168.55. For $C_{14}H_{10}N_2OS$ calcd. 66.12% C, 3.96% H, 11.02% N; found: 66.08% C, 3.96% H, 11.08% N. Mass (ESI), *m/z*: 255 (M+1).

3-[2-(Pyridin-3-yl)thiazol-4-yl]phenol (5)

Yield: 78%, mp: 193.2°C, IR υmax (cm^{-1}): 3173.3–2976 (aromatic C—H), 1274.60 (C—O). ^{1}H NMR (500 MHz) (DMSO-d_6) δ (ppm): 6.81 (dd, 1H, *J* = 2.24 Hz, *J* = 7.96 Hz, Ph), 7.29 (t, 1H, *J* = 7.80 Hz, *J* = 7.80 Hz, Ph), 7.48 (s, 1H, Ph), 7.50 (d, 1H, *J* = 8.6 Ar C6-H), 7.59 (dd, 1H, *J* = 4.77 Hz, *J* = 7.93 Hz, Py), 8.19 (s, 1H, Th), 8.38 (dt, 1H, *J* = 1.88 Hz, *J* = 1.88 Hz, *J* = 7.97 Hz, Py), 8.71 (dd, 1H, *J* = 1.39 Hz, *J* = 4.77 Hz, Py), 9.21 (d, 1H, *J* = 2.20 Hz, Py), 9.56 (s, 1H, OH). ^{13}C NMR: 113.60, 115.91, 117.50, 124.76, 129.51, 130.34, 134.11, 135.47, 147.41, 151.45, 156.11, 158.25, 164.20. For $C_{14}H_{10}N_2OS$ calcd. 66.12% C, 3.96% H, 11.03% N; found: 66.10% C, 3.95% H, 11.06% N. Mass (ESI) *m/z*: 255 (M+1).

3-[2-(Pyridin-4-yl)thiazol-4-yl]phenol (6)

Yield: 80%, mp: 234°C, IR υmax (cm^{-1}): 3556.37–2986.72 (aromatic C—H), 1262.25 (C—O). ^{1}H NMR (500 MHz) (DMSO-d_6) δ (ppm): 6.84 (dd, 1H, *J* = 2.24 Hz, *J* = 8.11 Hz, Ph), 7.31 (t, 1H, *J* = 8.08 Hz, *J* = 8.08 Hz, Ph), 7.50–7.52 (m, 2H, Ph), 8.26 (d, 2H, Py), 8.42 (s, 1H, Th), 8.90 (d, 2H, *J* = 4.42 Hz, Py), 9.62 (s, 1H, OH). ^{13}C NMR: 113.67, 116.25, 117.59, 119.01, 121.88, 130.44, 135.07, 143.39, 147.82, 157.04, 158.33, 163.13. For $C_{14}H_{10}N_2OS$ calcd. 66.12% C, 3.96% H, 11.03% N; found: 66.08% C, 3.97% H, 11.03% N. Mass (ESI) *m/z*: 255 (M+1).

4-[2-(Pyridin-2-yl)thiazol-4-yl]phenol (7)

Yield: 70%, mp: 148.2°C, IR υmax (cm^{-1}): 3109.26 (aromatic C—H), 1247.79 (C—O). ^{1}H NMR (500 MHz) (DMSO-d_6) δ (ppm): 6.88 (d, 2H, *J* = 8.57 Hz, Ph), 7.52 (dd, 1H, *J* = 4.93 Hz, *J* = 6.86 Hz, Py), 7.89 (d, 2H, *J* = 8.56 Hz, Ph), 7.99–8.02 (m, 2H, Py and Th), 8.24 (d, 1H, *J* = 7.87 Hz, Py), 8.66 (d, 1H, *J* = 4.73 Hz, Py), 9.66 (s, 1H, OH). ^{13}C NMR: 114.58, 116.02, 119.68, 125.57, 125.79, 127.99, 138.22, 150.18, 151.01, 156.48, 158.14, 168.33. For $C_{14}H_{10}N_2OS$ calcd. 66.12% C, 3.96% H, 11.02% N; found: 66.10% C, 3.95% H, 11.06% N. Mass (ESI) *m/z*: 255 (M+1).

4-[2-(Pyridin-3-yl)thiazol-4-yl]phenol (8)

Yield: 65%, mp: 252.8°C, IR υmax (cm^{-1}): 3093.77–2805.3 (aromatic C—H), 1257.70–1241.32 (C—O). ^{1}H NMR (500 MHz) (DMSO-d_6) δ (ppm): 6.87 (d, 2H, *J* = 8.68 Hz, Ph), 7.59 (dd, 1H, *J* = 4.69 Hz, *J* = 7.80 Hz, Py), 7.90 (d, 2H, *J* = 8.65 Hz, Ph), 8.02 (s, 1H, Th), 8.39 (d, 1H, *J* = 7.99 Hz, Py) 8.72 (s, 1H, Py), 9.23 (s, 1H, Py), 9.68 (s, 1H, OH). ^{13}C NMR: 113.13, 116.03, 124.83, 125.56, 128.14, 134.11, 147.30, 151.25, 156.38, 158.24, 163.95. For $C_{14}H_{10}N_2OS$ calcd. 66.12% C, 3.96% H, 11.02% N; found: 66.15% C, 3.97% H, 11.03% N. Mass (ESI) *m/z*: 255 (M+1).

4-[2-(Pyridin-4-yl)thiazol-4-yl]phenol (9)

Yield: 73%, mp: 252.8°C, IR umax (cm^{-1}): 3118–3006.76 (aromatic C—H), 1241.86 (C—O). ^{1}H NMR (500 MHz) (DMSO-d_6) δ (ppm): 6.88 (d, 2H, *J* = 8.57 Hz, Ph), 7.90 (d, 2H, *J* = 8.56 Hz, Ph), 7.97 (d, 2H, *J* = 4.70 Hz, Py and Ph), 8.11 (s, 1H, Th), 8.78 (d, 2H, Py), 9.70 (s, 1H, OH). ^{13}C NMR: 114.40, 116.07, 120.60, 125.42, 128.18, 140.13, 151.18, 156.77, 158.35, 164.39. For $C_{14}H_{10}N_2OS$ calcd. 66.12% C, 3.96% H, 11.01% N; found: 66.09% C, 3.98% H, 11.04% N. Mass (ESI) *m/z*: 255 (M+1).

4-Methyl-2-[2-(pyridin-2-yl)thiazol-4-yl]phenol (10)

Yield: 78.4%, mp: 167°C, IR umax (cm^{-1}): 3102–3048 (aromatic C—H), 2987–2914 (aliphatic C—H), 1246 (C—O). ^{1}H NMR (500 MHz) (DMSO-d_6) δ (ppm): 2.3 (s, 3H, CH_3), 6.8 (d, 1H, *J* = 8.1 Hz, Ph), 7.0 (dd, 1H, *J* = 2.0 Hz, *J* = 8.2 Hz, Ph), 7.55–7.52 (m, 1H, Py), 7.9 (d, 1H, *J* = 1.7 Hz, Ph), 8.0 (td, 1H, *J* = 1.6 Hz, *J* = 7.7 Hz, Py), 8.2 (d, 1H, *J* = 7.8 Hz, Py), 8.2 (s, 1H, Th), 8.6 (d, 1H, *J* = 4.1 Hz, Py), 10.2 (s, 1H, OH). ^{13}C NMR: 20.74, 116.87, 119.2, 119.78, 119.82, 125.70, 128.17, 129.15, 130.27, 138.32, 150.26, 150.71, 153.35, 167.24. For $C_{15}H_{12}N_2OS$ calcd. 67.14% C, 4.51% H, 10.44% N; found: 66.12% C, 4.33% H, 9.99% N. Mass (ESI), *m/z*: 269 (M+1).

4-Methyl-2-[2-(pyridin-3-yl)thiazol-4-yl]phenol (11)

Yield: 80.2%, mp: 217°C, IR umax (cm^{-1}): 3095, 3044, 3021 (aromatic C—H), 2919 (aliphatic C—H), 1251–1238 (C—O). ^{1}H NMR (500 MHz) (DMSO-d_6) δ (ppm): 2.3 (s, 3H, CH_3), 6.9 (d, 1H, *J* = 8.1 Hz, Ph), 7.03 (dd, 1H, *J* = 2.0 Hz, *J* = 8.1 Hz, Ph), 7.76–7.73 (m, 1H, Py), 8.0 (d, 1H, *J* = 1.7 Hz, Ph), 8.3 (s, 1H, Th), 8.6 (d, 1H, *J* = 6.4 Hz, Py), 8.7 (d, 1H, *J* = 4.4 Hz, Py), 9.3 (s, 1H, Py), 10.3 (s, 1H, OH). ^{13}C NMR: 20.72, 116.83, 118.54, 119.68, 125.65, 128.18, 129.45, 130.12, 130.41, 136.40, 145.64, 149.30, 153.24, 153.37, 161.94. For $C_{15}H_{12}N_2OS$ calcd. 67.14% C, 4.51% H, 10.44% N; found: 66.87% C, 4.13% H, 9.31% N. Mass (ESI), *m/z*: 269 (M+1).

4-Methyl-2-[2-(pyridin-4-yl)thiazol-4-yl]phenol (12)

Yield: 79.3%, mp: 184.5°C, IR umax (cm^{-1}): 3106–3031 (aromatic C—H), 2913 (aliphatic C—H), 1238 (C—O). ^{1}H NMR (500 MHz) (DMSO-d_6) δ (ppm): 2.3 (s, 3H, CH_3), 6.9 (d, 1H, *J* = 8.2 Hz, Ph), 7.0 (dd, 1H, *J* = 1.8 Hz, *J* = 8.1 Hz, Ph), 7.9 (d, 2H, *J* = 6.0 Hz, Ph), 8.0 (d, 1H, *J* = 1.6 Hz, Ph), 8.3 (s, 1H, Th), 8.7 (d, 2H, *J* = 6.0 Hz, Py), 10.3 (s, 1H, OH). ^{13}C NMR: 20.72, 116.83, 119.19, 119.71, 120.57, 128.21, 129.45, 130.45, 139.86, 151.28, 153.38, 153.46, 163.23. For $C_{15}H_{12}N_2OS$ calcd. 67.14% C, 4.51% H, 10.44% N; found: 66.31% C, 3.99% H, 10.31% N. Mass (ESI), *m/z*: 269 (M+1).

4-Methoxy-2-[2-(pyridin-2-yl)thiazol-4-yl]phenol (13)

Yield: 79.8%, mp: 142.8°C, IR umax (cm^{-1}): 3076 (aromatic C—H), 2981 (aliphatic C—H), 1222 (C—O). ^{1}H NMR (500 MHz) (DMSO-d_6) δ (ppm): 3.8 (s, 3H, OCH_3), 6.8 (dd, 1H, *J* = 3.1 Hz, *J* = 8.8 Hz, Ph), 6.9 (d, 1H, *J* = 8.8 Hz, Ph), 7.54–7.52 (m, 1H, Py), 7.7 (d, 1H, *J* = 3.0 Hz, Ph), 8.0 (td, 1H, *J* = 1.7 Hz, *J* = 7.7 Hz, Py), 8.2 (d, 1H, *J* = 7.8 Hz, Py), 8.3 (s, 1H, Th), 8.6 (d, 1H, *J* = 3.6 Hz, Py), 10.1 (s, 1H, OH). ^{13}C NMR: 55.9, 113.52, 115.76, 117.71, 119.79, 119.82, 120.43, 125.72, 138.31, 149.57, 150.24, 150.67, 152.70, 153.08, 167.28. For $C_{15}H_{12}N_2O_2S$ calcd. 63.36% C, 4.25% H, 9.85% N; found: 62.78% C, 3.83% H, 9.76% N. Mass (ESI), *m/z*: 285 (M+1).

4-Methoxy-2-[2-(pyridin-3-yl)thiazol-4-yl]phenol (14)

Yield: 81.3%, mp: 167°C, IR umax (cm^{-1}): 3063 (aromatic C—H), 2944–2906 (aliphatic C—H), 1221 (C—O). ^{1}H NMR (500 MHz) (DMSO-d_6) δ (ppm): 3.7 (s, 3H, OCH_3), 6.8 (dd, 1H, *J* = 3.1 Hz, *J* = 8.8 Hz, Ph), 6.9 (d, 1H, *J* = 8.8 Hz, Ph), 7.60–7.57 (m, 1H, m, Py), 7.7 (d, 1H, *J* = 3.11 Hz, Ph), 8.3 (s, 1H, Th), 8.4 (d, 1H, *J* = 5.9 Hz, Py), 8.7 (d, 1H, *J* = 3.3 Hz, Py), 9.2 (s, 1H, Py), 10.1 (s, 1H, OH). ^{13}C NMR: 55.9, 113.68, 115.89, 117.69, 118.40, 120.35, 124.77, 129.27, 134.17, 147.47, 149.57, 151.48, 152.69, 152.88, 163.17. For $C_{15}H_{12}N_2O_2S$ calcd. 63.36% C, 4.25% H, 9.85% N; found: 63.05% C, 4.18% H, 9.70% N. Mass (ESI), *m/z*: 285 (M+1).

4-Methoxy-2-[2-(pyridin-4-yl)thiazol-4-yl]phenol (15)

Yield: 78.6%, mp: 153.4°C, IR umax (cm^{-1}): 3124–3065 (aromatic C—H), 2951 (aliphatic C—H), 1215 (C—O). ^{1}H NMR (500 MHz) (DMSO-d_6) δ (ppm): 3.7 (s, 3H, OCH_3), 6.8 (dd, 1H, *J* = 3.1 Hz, *J* = 8.8 Hz, Ph), 6.9 (d, 1H, *J* = 8.8 Hz, Ph), 7.7 (d, 1H, *J* = 3.12 Hz, Ph), 7.9 (d, 2H, *J* = 6.0 Hz, Py), 8.4 (s, 1H, Th), 8.7 (d, 2H, *J* = 4.6 Hz, Py), 10.1 (s, 1H, OH). ^{13}C NMR: 55.9, 113.78, 115.96, 117.70, 119.69, 120.34, 120.57, 139.81, 149.60, 151.28, 152.70, 153.20, 163.29. For $C_{15}H_{12}N_2O_2S$ calcd. 63.36% C, 4.25% H, 9.85% N; found: 62.77% C, 3.90% H, 9.31% N. Mass (ESI), *m/z*: 285 (M+1).

4-Chloro-2-[2-(pyridin-2-yl)thiazol-4-yl]phenol (16)

Yield: 79.5%, mp: 193.7°C, IR umax (cm^{-1}): 3105 (aromatic C—H), 1247 (C—O). ^{1}H NMR (500 MHz) (DMSO-d_6) δ (ppm): 7.0 (d, 1H, *J* = 8.6 Hz, Ph), 7.2 (dd, 1H, *J* = 2.7 Hz, *J* = 8.6 Hz, Ph), 7.54–7.52 (m, 1H, m, Py), 8.0 (td, 1H, *J* = 1.6 Hz, *J* = 7.6 Hz, Py), 8.2 (d, 1H, *J* = 2.7 Hz, Ph), 8.2 (d, 1H, *J* = 7.8 Hz, Py), 8.3 (s, 1H, Th), 8.6 (d, 1H, *J* = 4.7 Hz, Py), 10.7 (s, 1H, OH). ^{13}C NMR: 118.61, 119.94, 120.91, 122.10, 123.41, 125.77, 128.30, 129.07, 138.30, 150.22, 150.64, 151.47, 154.40, 167.51. For $C_{14}H_9ClN_2OS$ calcd. 58.23% C, 3.14% H, 9.70% N; found: 57.34% C, 2.90% H, 9.45% N. Mass (ESI), *m/z*: 289 (M+1).

4-Chloro-2-[2-(pyridin-3-yl)thiazol-4-yl]phenol (17)

Yield: 80.3%, mp: 179.3°C, IR umax (cm^{-1}): 3094–3041 (aromatic C—H), 1246 (C—O). ^{1}H NMR (500 MHz) (DMSO-d_6) δ (ppm): 7.0 (d, 1H, *J* = 8.67 Hz, Ph), 7.2 (dd, 1H, *J* = 2.7 Hz, *J* = 8.6 Hz, Ph), 7.59–7.56 (m, 1H, Py), 8.2 (d, 1H, *J* = 2.6 Hz, Ph), 8.3 (s, 1H, Th), 8.4 (d, 1H, *J* = 9.7 Hz, Py), 8.7 (d, 1H, *J* = 4.7 Hz, Py), 9.2 (s, 1H, Py), 10.7 (s, 1H, OH). ^{13}C NMR: 118.58, 119.50, 121.97, 123.41, 124.75, 128.51, 129.18, 129.22, 134.22, 147.53, 151.29, 151.53, 154.40, 163.17. For $C_{14}H_9ClN_2OS$ calcd. 58.23% C, 3.14% H, 9.70% N; found: 57.78% C, 2.99% H, 9.21% N. Mass (ESI), *m/z*: 289 (M+1).

4-Chloro-2-[2-(pyridin-4-yl)thiazol-4-yl]phenol (18)

Yield: 78.5%, mp: 203.6°C, IR umax (cm^{-1}): 3032 (aromatic C—H), 1254 (C—O). ^{1}H NMR (500 MHz) (DMSO-d_6) δ (ppm): 7.0 (d, 1H, *J* = 8.6 Hz, Ph), 7.2 (dd, 1H, *J* = 2.7 Hz, *J* = 8.6 Hz, Ph), 7.9 (d, 2H, *J* = 6.0 Hz Py), 8.2

(d, 1H, *J* = 2.7 Hz, Ph), 8.4 (s, 1H, Th), 8.7 (d, 2H, *J* = 4.6 Hz, Py), 10.7 (s, 1H, OH). ^{13}C NMR: 118.60, 120.66, 120.88, 121.95, 123.42, 128.55, 129.30, 139.75, 151.29, 151.60, 154.43, 163.58. For $C_{14}H_9ClN_2OS$ calcd. 58.23% C, 3.14% H, 9.70% N; found: 57.77% C, 2.95% H, 9.55% N. Mass (ESI), *m/z*: 289 (M+1).

3.2 | Pharmacology

3.2.1 | Aromatase activity assay

Aromatase inhibition is quantified by measuring the fluorescent intensity of fluorescein, the hydrolysis product of dibenzylfluorescein, by aromatase. With slight modification to the method described by Stresser,[34] experiments were carried out following the instructions provided by the "CYP19/MFC High Throughput Inhibitor Screening assay kit" (Corning, Catalog number: 459520). Stock solutions of the compounds were prepared with DMSO (1%). In brief, the test substance (10 µM) and the standard solution [3 µL HFC (7-hydroxy-4-trifluoromethyl coumarone 0.25 M), 147 µL NADPH-Cofactor Mix without acetonitrile] were preincubated with the NADPH regenerating system (1.3 mM $NADP^+$, 66 mM glucose 6-phosphate dehydrogenase, 66 mM $MgCl_2$) for 10 min at 37°C. Then, 100 µL of the enzyme and substrate mixture [1 µM enzyme (CYP19), 25 mM 7-methoxy-4-trifloromethyl coumarone and 0.5 M phosphate buffer, pH 7.4] were added. The reaction mixture was incubated for 30 min at 37°C to allow aromatase to generate the product and the reaction was quenched with a stop reagent, 0.5 M Tris base. After the reaction was terminated, fluorescence was measured at 409 nm (excitation) and 530 nm (emission). Experiments were performed in triplicate and the average values were used to construct the dose–response curves. GraphPad Prism software Version 7.02 (La Jolla, California, USA) was used to calculate the IC_{50} values of a minimum of eight concentrations of each test substance (Table 3).

3.2.2 | Evaluation of anticancer activity against MCF7 and HEK 293 cells

MTT (3-[4,5-dimethylthiazol-2-yl]-2,5-diphenyltetrazolium bromide) is a water soluble tetrazolium salt. The MTT assay was discovered by Mosmann (1983).[35] In this colorimetric technique, the tetrazolium ring is converted to an insoluble purple formazan by cleavage of that ring by increased activity of succinate dehydrogenase on live cells within the mitochondria. Experiments were carried out following the instructions given in "Cell Proliferation Kit I (MTT)" (Roche, Catalog Number: 11 465 007 001). The effects of tested compounds on cell viability of the human breast adenocarcinoma cell line (MCF7) and human embryonic kidney cell line (HEK 293) were determined using this colorimetric technique. MCF7 and HEK 293 cells were cultured in 96-well plates in 100 µL of Dulbecco's Modified Eagle's Medium (GIBCO, UK) with 10% of charcoal stripped fetal bovine serum (GIBCO, UK), 1% penicillin-streptomycin (GIBCO, UK), 1% L-glutamine (GIBCO, UK) per well at a cell density of 5×10^4 cell/wells. Experiment sets of

TABLE 3 Calculated drug-likeness, molecular properties, and ADME predictions for the active compounds using QikProp

Compound	#stars	CNS	logPo/w	logHERG	PCaco	logBB	PMDCK	log K_p	log K_{HSA}	HOA[a]	%HOA
1	0.00	1.00	3.28	−5.59	2993.15	0.13	2876.81	−1.07	0.18	3.00	100.00
2	0.00	0.00	2.95	−5.48	2149.23	−0.02	1923.02	−1.40	0.08	3.00	100.00
3	0.00	1.00	2.95	−5.46	2233.53	0.00	2009.79	−1.36	0.08	3.00	100.00
4	0.00	0.00	3.16	−5.64	1900.06	−0.07	1743.99	−1.50	0.19	3.00	100.00
5	0.00	0.00	2.82	−5.52	1411.73	−0.20	1221.57	−1.80	0.09	3.00	100.00
6	0.00	0.00	2.82	−5.52	1413.03	−0.20	1224.67	−1.80	0.09	3.00	100.00
7	1.00	0.00	3.17	−5.64	1894.97	−0.08	1738.77	−1.50	0.19	3.00	100.00
8	0.00	0.00	2.83	−5.53	1406.67	−0.20	1216.28	−1.80	0.09	3.00	100.00
9	0.00	0.00	2.83	−5.53	1408.05	−0.20	1220.20	−1.80	0.09	3.00	100.00
10	0.00	1.00	3.44	−5.55	2980.62	0.11	2864.81	−1.27	0.33	3.00	100.00
11	0.00	0.00	3.22	−5.43	2228.99	−0.02	2002.83	−1.56	0.23	3.00	100.00
12	0.00	0.00	3.22	−5.43	2223.69	−0.02	2000.72	−1.56	0.23	3.00	100.00
13	0.00	1.00	3.34	−5.49	2989.42	0.05	2848.85	−1.17	0.19	3.00	100.00
14	0.00	0.00	3.03	−5.41	2115.32	−0.10	1899.45	−1.51	0.10	3.00	100.00
15	0.00	0.00	3.03	−5.38	2238.54	−0.07	2015.03	−1.46	0.09	3.00	100.00
16	0.00	1.00	3.70	−5.55	2979.05	0.29	7046.34	−1.24	0.29	3.00	100.00
17	1.00	1.00	3.36	−5.42	2227.58	0.16	4927.40	−1.53	0.19	3.00	100.00
18	0.00	1.00	3.36	−5.42	2225.93	0.16	4930.27	−1.53	0.19	3.00	100.00

[a]The assessment uses a knowledge-based set of rules including checking for suitable values for the percent of human oral absorption, number of metabolites, number of rotatable bonds, logP, solubility, and cell permeability.

different concentrations were prepared. Control wells were formed by preparing culture media without compounds. The cells were incubated for 24 h (37°C and 5% CO_2). Following this step, each medium in wells was changed with fresh medium and different concentrations of compounds was added and incubated for 6 h. After incubation, 10 µL of MTT (final concentration 0.5 mg/mL) was added and left for 4 h. A total of 100 µL of a solubilization solution containing 10% SDS in 0.01 M HCl was added into each well. Absorbance at 550 nm was recorded with an ELISA plate reader.[36,37] Each set of experiments was performed in triplicate.

3.3 | Molecular modeling studies

3.3.1 | Ligand preparation and docking experiment

The 3D diagrams of the synthesized compounds were drawn using the 3D builder implemented in the Maestro suite (Schrödinger LCC, Oregon, USA). The ligands were prepared and minimized by means of the OPLS_2005 force field and the partial atomic charges, ionization, and tautomerization states were computed at a pH range of 6–8 by Epik v1620716 using the LigPrep module of the same suite.

The most active compound found using the methods of the aromatase inhibition assay, 3-[2-(pyridin-4-yl)thiazol-4-yl]phenol (compound **6**), was subjected to a series of docking experiments to identify the probable interactions between the ligand and the aromatase active site. The preparation of the protein structure and ligand, GRID files, docking, and scoring were performed using algorithms included in the Maestro modules (Schrodinger Inc, USA). The X-ray crystallographic structure of human placental aromatase (PDB entry code: 3EQM) was obtained from the Protein Data Bank (RCSB).[7] The 3EQM PDB file was edited using the protein preparation wizard from the Workflows menu (Maestro) for hydrogen insertion and rotamer adjustment, and H-bond optimization using OPLS 2005 as the energy parameters. Ligand docking was performed with the Glide module in Schrodinger. Extra Precision (XP) and induced-fit protocols included in Glide were employed with the parameter settings recommended by Caporuscio et al.[29] for docking studies.

3.3.2 | Prediction of drug-likeness, molecular and ADME properties

For all the synthesized molecules, the ADME properties (46 molecular descriptors) were determined using the QikProp program (Schrödinger 2016-4) in the normal mode. QikProp generates physically relevant descriptors and uses them to perform ADME predictions. An overall ADME-compliance score representing the drug-likeness parameter (indicated by #stars) was used to assess the pharmacokinetic profiles of the compounds. The #stars parameter (ranging from 0 to 5) indicates the number of property descriptors computed by QikProp that fall outside the optimum range values for 95% of known drugs. The predicted descriptors were central nervous system (CNS) activity (−2 for inactive to +2 for active); octanol/water partition coefficient, logPo/w (−2.0 to 6.5); the IC_{50} value for the block of HERG K^+ channels, logHERG (concern <−5); Caco-2 cell membrane permeability in nm/s, PCaco (<5 low to >100 high); the logarithm of the predicted blood/brain barrier (BBB) partition coefficient, logBB (−3.0 to 1.0); apparent Madin–Darby canine kidney cell permeability (PDMCK) that mimics BBB for non-active transport in nm/s, PMDCK (<25 poor to >500 great); skin permeability, log K_p (−8.0 to −1.0); the logarithm of binding constant to human serum albumin, log K_{HSA} (−1.5 to 1.2); qualitative human oral absorption (HOA) (1: low, 2: medium, 3: high); and percent of HOA (>80%: high, <25%: poor).

ACKNOWLEDGMENT

This study was supported by Anadolu University Scientific Research Projects Commission (Project No: 1410S422).

CONFLICT OF INTEREST

The authors declare no conflict of interest.

ORCID

Merve Ertas http://orcid.org/0000-0002-2289-7950
Leyla Yurttas http://orcid.org/0000-0002-0957-6044

REFERENCES

[1] D. M. Parkin, F. Bray, J. Ferlay, P. Pisani, *CA Cancer J. Clin.* **2005**, *55*, 74.
[2] D. M. Barnes, R. R. Millis, C. E. Gillett, K. Ryder, D. Skilton, I. S. Fentiman, R. D. Rubens, *Endocr. Relat. Cancer* **2004**, *11*, 85.
[3] H. J. Huang, P. Neven, M. Drijkoningen, R. Paridaens, H. Wildiers, E. Van Limbergen, P. Berteloot, F. Amant, I. Vergote, M. R. Christiaens, *J. Clin. Pathol.* **2005**, *58*, 611.
[4] J. Fishman, J. Goto, *J. Biol. Chem.* **1981**, *256*, 4466.
[5] A. M. Brodie, W. C. Schwarzel, H. J. Brodie, *J. Steroid Biochem.* **1976**, *7*, 787.
[6] W. R. Miller, *Br. J. Cancer* **1996**, *73*, 415.
[7] D. Ghosh, J. Griswold, M. Erman, W. Pangborn, *Nature* **2009**, *457*, 219.
[8] J. M. Nabholtz, A. Buzdar, M. Pollak, W. Harwin, G. Burton, A. Mangalik, M. Steinberg, A. Webster, M. Von Euler, *J. Clin. Oncol.* **2000**, *18*, 3758.
[9] H. Mouridsen, M. Gershanovich, Y. Sun, R. Perez-Carrion, C. Boni, A. Monnier, J. Apffelstaedt, R. Smith, H. P. Sleeboom, F. Janicke, A. Pluzanska, M. Dank, D. Becquart, P. P. Bapsy, E. Salminen, R. Snyder, M. Lassus, J. A. Verbeek, B. Staffler, H. A. Chaudri-Ross, M. Dugan, *J. Clin. Oncol.* **2001**, *19*, 2596.
[10] P. E. Lønning, J. Geisler, *Expert Opin. Investig. Drugs* **2008**, *17*, 723.
[11] W. R. Miller, *Cancer Treat. Rev.* **1989**, *16*, 83.
[12] X. J. Yi, T. T. El-Idreesy, T. M. Eldebss, A. M. Farag, M. M. Abdulla, S. A. Hassan, Y. N. Mabkhot, *Chem. Biol. Drug Des.* **2016**, *88*, 832.
[13] F. Orsini, L. Verotta, K. Klimo, C. Gerhauser, *Arch. Pharm. (Weinheim)* **2016**, *349*, 414.
[14] Y. Dai, S. Ziyue, S. Liu, Q. Cui, T. Zhang, X. Zhang, *J. Chem. Pharm. Res.* **2015**, *7*, 706.
[15] I. Thomas, J. A. Carter, *Br. J. Anaesth.* **2006**, *6*, 182.
[16] T. Ogas, T. P. Kondratyuk, J. M. Pezzuto, *Ann. NY Acad. Sci.* **2013**, *1290*, 21.

[17] A. S. Mayhoub, L. Marler, T. P. Kondratyuk, E. J. Park, J. M. Pezzuto, M. Cushman, *Bioorg. Med. Chem.* **2012**, *20*, 7030.
[18] A. S. Mayhoub, L. Marler, T. P. Kondratyuk, E. J. Park, J. M. Pezzuto, M. Cushman, *Bioorg. Med. Chem.* **2012**, *20*, 510.
[19] A. S. Mayhoub, L. Marler, T. P. Kondratyuk, E. J. Park, J. M. Pezzuto, M. Cushman, *Bioorg. Med. Chem.* **2012**, *20*, 2427.
[20] L. D. C. Arnold, W. Jotham, T. Kaneko, M. P. Moyer, Pfizer Inc., U.S.A.: U.S., **1994**.
[21] L. D. Arnold, J. W. Coe, T. Kaneko, M. P. Moyer, Pfizer Inc., U. S., **2000**.
[22] R. F. Day, J. A. Lafontaine, Google Patents: **2002**.
[23] H. Ito, S. Hitoshi, Y. Miki, T. Hayashi, M. Iwata, M. Yamaki, Jpn. Kokai Tokkyo Koho, **1995**.
[24] H. Ito, S. Hitoshi, Y. Miki, T. Hayashi, M. Iwata, M. Yamaki, Hitachi Chemical Co Ltd, Japan: **1996**.
[25] H. Ito, S. Hitoshi, Y. Miki, T. Hayashi, M. Iwata, M. Yamaki, Kokai Tokkyo Koho: **1996**.
[26] K. Kondo, S. Takashi, Takeda Chemical Industries, **1990**.
[27] R. H. Vekariya, H. D. Patel, *Tetrahedron Lett*. **2014**, *70*, 3949.
[28] A. Weissberger, E. C. Taylor, in *The Chemistry of Heterocyclic Compounds*, Vol. 34 (Ed: J. V. Metzger), Wiley, New York **1979**.
[29] F. Caporuscio, G. Rastelli, C. Imbriano, A. Del Rio, *J. Med. Chem*. **2011**, *54*, 4006.
[30] B. Testa, P. Jenner, *Drug Metab. Rev*. **1981**, *12*, 1.
[31] J. I. Vandenberg, B. D. Walker, T. J. Campbell, *Trends Pharmacol. Sci*. **2001**, *22*, 240.
[32] N. Chiesa, B. Rosati, A. Arcangeli, M. Olivotto, E. Wanke, *J. Physiol. (Cambridge, U. K.)* **1997**, *501*, 313.
[33] A. M. Aronov, *Drug Discov. Today* **2005**, *10*, 149.
[34] D. M. Stresser, S. D. Turner, J. McNamara, P. Stocker, V. P. Miller, C. L. Crespi, C. J. Patten, *Anal. Biochem*. **2000**, *284*, 427.
[35] T. Mosmann, *J. Immunol. Methods* **1983**, *65*, 55.
[36] X. Shi, M. Sun, H. Liu, Y. Yao, R. Kong, F. Chen, Y. Song, *Mol. Carcinog*. **2015**, *54*(Suppl 1), E1.
[37] J. H. Park, S. J. Kim, E. J. Oh, S. Y. Moon, S. I. Roh, C. G. Kim, H. S. Yoon, *Biol. Reprod*. **2003**, *69*, 2007.

SUPPORTING INFORMATION

Additional Supporting Information may be found online in the supporting information tab for this article.

How to cite this article: Ertas M, Sahin Z, Berk B, Yurttas L, Biltekin SN, Demirayak S. Pyridine-substituted thiazolylphenol derivatives: Synthesis, modeling studies, aromatase inhibition, and antiproliferative activity evaluation. *Arch Pharm Chem Life Sci*. 2018;1–11. https://doi.org/10.1002/ardp.201700272